

Evolution in the clustering strength of radio galaxies

S. Fine^{1*}, T. Shanks¹, N. Nikoloudakis¹, U. Sawangwit¹

¹*Department of Physics, Durham University, South Road, Durham DH1 3LE, UK*

27 September 2018

ABSTRACT

We cross match the NVSS and FIRST surveys with three large photometric catalogues of luminous red galaxies (LRGs) to define radio-loud samples. These have median redshifts 0.35, 0.55 and 0.68 and, by matching rest-frame optical and radio properties, we construct uniform samples across the three surveys. This paper is concerned with the clustering properties of these samples derived from the angular correlation function. The primary aim is to characterise any evolution in the clustering amplitude of radio galaxies below $z \sim 0.68$.

We find no evidence for evolution in the large-scale ($\sim 1 - 50 h^{-1}$ Mpc) clustering amplitude. Our radio galaxy autocorrelations are consistent with previous findings indicating little-to-no evolution in the redshift range 0.68 to 0 (~ 6 Gyr of time). We also cross correlate radio galaxies with the parent LRG samples to increase the precision of our results and again find no evidence for evolution in comoving coordinates. Our results are inconsistent with a long-lived model for the clustering evolution that assumes radio sources randomly sample the LRG population. A model where the halo mass is constant with redshift is consistent with the data. This is similar to QSOs that have clustering amplitudes consistent with a single halo mass at all redshifts. Given that the brightest radio sources show stronger evolution in space density compared to fainter radio sources we restrict our samples to include only objects with $L > 10^{26}$ W/Hz and repeat the analysis. Again we find no evidence for evolution in the comoving correlation amplitude. These radio sources appear to inhabit the same mass halos as fainter radio galaxies ($\sim 9 \times 10^{13} h^{-1} M_{\odot}$). These halos are \sim twice as massive as those of the general LRG population ($\sim 4 \times 10^{13} h^{-1} M_{\odot}$) and ~ 30 times as massive as optical AGN/QSOs ($\sim 3 \times 10^{12} h^{-1} M_{\odot}$).

Key words: galaxies: active ; Galaxies z galaxies: evolution ; Galaxies z

1 INTRODUCTION

Radio galaxies have long been used to study large scale structure as they are highly biased indicators of the mass distribution and are naturally found in the high redshift ($z \sim 1$) Universe. Understanding the observed bias of radio galaxies requires relating their clustering to that of their host populations. Furthermore, any differential evolution in their clustering with respect to their hosts gives insight into the nature of radio galaxies and the mechanisms that trigger them.

The typical host galaxy of a radio source depends strongly on its luminosity. At lower radio luminosities ($L \lesssim 10^{23}$ W/Hz) the population is almost exclusively made up of starforming galaxies with related diffuse radio emission, above $L \sim 10^{23}$ W/Hz almost all radio sources are

associated with active galactic nuclei (AGN). The hosts of the brightest radio galaxies have strong emission lines (e.g. Hine & Longair 1979; McCarthy 1993) while lower-luminosity radio AGN are hosted by massive ellipticals with little-to-no optical line emission. This transition implies a cutoff luminosity between objects with and without emission lines that Johnston et al. (2008) found to be around $\sim 10^{26}$ W/Hz. This luminosity is close to the traditional cutoff between morphologically classified FRI and FRII objects (Fanaroff & Riley 1974). Furthermore, while the bright end of the radio luminosity function evolves strongly towards higher space densities at high z (Longair 1966; Dunlop & Peacock 1990), fainter radio AGN ($L \lesssim 10^{26}$ W/Hz) show much less evidence for evolution (Clewley & Jarvis 2004; Sadler et al. 2007). This evolution in space density is roughly matched by the typical hosts of radio AGN. Massive elliptical galaxies (luminous red galaxies; LRGs), that host lower luminosity radio AGN, show lit-

* stephen.fine@durham.ac.uk

the evolution in number density for $z < 1$ (Bell et al. 2004; Wake et al. 2006; Brown et al. 2007). Higher luminosity radio sources are more associated with optical/Xray AGN (McCarthy 1993) that show strong evolution out to $z \sim 2.5$ (Schmidt 1968; Croom et al. 2009).

Radio sources are strongly biased tracers of the underlying mass distribution of the Universe (Yates et al. 1989; Peacock & Nicholson 1991; Blake & Wall 2002; Magliocchetti et al. 2004; Brand et al. 2005). Since the advent of deep all sky surveys (e.g. FIRST, NVSS, SUMSS, WENSS) there have been major leaps in the ability to describe the environments of radio galaxies. These milli-Jansky surveys sample the luminosity range $\sim 10^{23}$ to 10^{26} W/Hz at moderate redshifts, where radio sources are found almost exclusively in LRGs. LRGs are known to be a strongly biased tracer of the matter density, and their bias increases with the mass/luminosity of the LRG.

Radio sources tend to be found in the most massive elliptical galaxies and more massive galaxies are more likely to host them (Best et al. 2005; Mauch & Sadler 2007). Recent studies have compared the clustering of radio galaxies to that of radio-quiet galaxies that have been matched in their optical properties to the radio sample. Most find that radio galaxies are significantly more clustered than optically identical samples of quiescent galaxies (Wake et al. 2008; Mandelbaum et al. 2009; Donoso et al. 2009), although see Hickox et al. (2009) for a counter example we will discuss later. The indication is that the environment of a galaxy contributes to the probability of it hosting a radio source.

In this paper we are primarily concerned with how the clustering of radio sources evolves for $z \lesssim 0.7$. In this redshift interval the clustering amplitude of LRGs is approximately constant (Wake et al. 2008; Sawangwit et al. 2009). However, the clustering amplitude of quasars evolves such that, when models of gravitational collapse are assumed, the implied dark halo mass for quasars is approximately constant (Croom et al. 2005; Ross et al. 2009). We will evaluate the clustering amplitude of radio LRGs in a series of samples from $z \sim 0.68$ to 0.35 to investigate any evolution in their clustering. This will be done both for a sample of medium luminosity ($L \sim 10^{24.7}$ W/Hz) radio galaxies, and a high luminosity subsample ($L > 10^{26}$ W/Hz).

In section 2 we introduce the data that will be used in this work, section 3 describes the algorithm we develop for identifying radio LRGs, section 4 describes the correlation analysis to be used, section 5 compares the clustering of radio-loud and quiet LRGs, section 6 then looks at the evolution of radio LRGs and in section 7 we investigate the evolution of the very brightest radio LRGs. Throughout this paper we assume a flat $(\Omega_m, \Omega_\Lambda) = (0.3, 0.7)$, $H_0 = 70 \text{ km s}^{-1} \text{ Mpc}^{-1}$ cosmology. All radio flux densities and luminosities are at 1.4 GHz unless otherwise stated and when estimating radio luminosities throughout this paper k -corrections have been performed assuming a continuum shape of $S_\nu \propto \nu^{-0.7}$.

2 DATA

The LRG samples used in this paper are originally defined from three spectroscopic surveys: SDSS, 2SLAQ and AAΩ (Eisenstein et al. 2001; Cannon et al. 2006; Ross et al.

2008). The LRG selection was refined by Sawangwit et al. (2009) to create photometric samples from the SDSS DR5 (York et al. 2000; Adelman-McCarthy et al. 2007) and to cut down on stellar contamination. We use LRG samples defined identically but drawn from the more recent DR7 (Abazajian et al. 2009).

To identify radio-loud LRGs in our sample we compare our LRG catalogues with radio source catalogues from the NVSS (Condon et al. 1998) and FIRST (Becker et al. 2000) surveys. Both surveys are carried out at 1.4 GHz and the high angular resolution (~ 5 arcsec) and faint flux limit ($1\sigma \sim 0.15 \text{ mJy}$) of the FIRST survey combined with the large-scale sensitivity of the NVSS make them complementary tools for identifying radio LRGs. The FIRST survey covers much of the same sky area as the SDSS north Galactic cap. In the overlap region there are 110104, 652401 and 799519 objects in the SDSS, 2SLAQ and AAΩ LRG samples respectively. See Sawangwit et al. (2009) for the redshift distributions, expected contamination and autocorrelation clustering properties of the LRG samples.

3 RADIO CROSS MATCHING

Complex radio source morphology due to extended structures compounded by size-dependent response effects due to the use of interferometers makes radio source matching more involved than simply matching sky positions. The most accurate and precise method for cross-matching has always been manual inspection (e.g. Sadler et al. 2007). However, the size of our LRG samples forces us to define an automated cross-matching procedure that does not require visual inspection of all of the potential radio matches in the sample. Automated radio-matching routines have been developed before (e.g. Best et al. 2005; Kimball & Ivezić 2008), and even samples defined by manual inspection use some automated procedures to define a sample of potential matches that are then visually inspected.

3.1 Our cross-matching procedure

Sadler et al. (2007) define two samples of radio LRGs from the 2SLAQ spectroscopic sample. One is based on manual inspection and the other based on automatic cross matching to the FIRST survey. We modified their selection criteria to define a radio matching procedure and use their manually inspected sample to test our results. We match the LRG and FIRST catalogues within a 30 arcsec radius, and the LRG and NVSS catalogues within a 180 arcsec radius, retaining all radio matches within the given radius around an LRG. In this initial cross matching we do not apply any radio flux limits, these are applied below. Following Sadler et al. (2007) we use the FIRST matches as our primary tool for identifying radio galaxies. We accept matches that meet one of three criteria:

- i*) A FIRST match is within 3 arcsec of the LRG position.
- ii*) A FIRST match is within 10 arcsec of the LRG position and the major axis of the source is orientated within 25° of the angle to the LRG position.
- iii*) Given more than one radio match, the flux-weighted mean of the FIRST positions (or any subset thereof) is within 6 arcsec of the LRG position.

For any sources that had NVSS matches within 180 arcsec but not FIRST matches we applied a similar set of criteria based on Best et al. (2005) to the NVSS sources to define potential radio galaxies. These are:

- i) An NVSS match is within 10 arcsec of the LRG position.
- ii) A galaxy matched to two radio components that is < 10 arcsec from the flux weighted radio centroid, and the radio-galaxy-radio angle is $> 150^\circ$
- iii) Given more than two radio matches, the flux-weighted mean of the NVSS positions is within 10 arcsec of the LRG position.

We apply this procedure to the 2SLAQ spectroscopic catalogue and find 428 objects satisfy our selection criteria. Of these, 57 objects do not appear in the Sadler catalogue, while 20 objects from the Sadler catalogue are not found. This indicates that we are $\sim 5\%$ incomplete with respect to the Sadler catalogue, the majority of sources missed by our selection criteria have complex structures in their FIRST images. Of the 57 extra matches 29 can be explained as objects that had NVSS matches but no corresponding FIRST sources. These objects were rejected by Sadler et al. to improve the reliability of their catalogue. We take an approach more similar to Best et al. (2005) including these sources given the criteria above. This indicates that our routine, applied to the 2SLAQ spectroscopic LRG catalogue, is $\sim 93\%$ reliable.

We apply this radio cross-matching routine to the SDSS, 2SLAQ and AA Ω photometric LRG samples and obtain 9689, 15236 and 8364 radio LRGs from the three samples. This corresponds to 8.8, 2.3 and 1.0% of the parent samples. The considerably higher detection rate for the SDSS sample is due to the lower redshift and higher absolute (optical) magnitude of the SDSS LRGs

We perform a simple check of the reliability of our final radio samples by offsetting the original LRG samples, then rerunning the cross-matching code on the offset catalogues. We offset the samples by $\pm 0.1^\circ$ in declination (twice the 180 arcsec maximum cross-matching radius used). The cross-matching code found 171/138, 516/453, 457/499 matches in the offset SDSS, 2SLAQ and AA Ω samples respectively for the positive and negative offsets. This corresponds to $\sim 1.5\text{-}6\%$ contamination in our final catalogues similar to the $\sim 7\%$ value found when comparing to Sadler et al. (2007).

Many of the radio identifications are based solely on matching to FIRST source catalogues thanks to the angular resolution of the FIRST survey. However, the FIRST survey's smaller beam resolves out large-scale structure and does not give accurate radio powers for these sources. We cross match our final radio LRG catalogue with the NVSS within a 180 arcsec radius. We then identify which NVSS matches are associated with the galaxy using the criteria above. We sum these NVSS components to give the radio flux densities used throughout this paper. The NVSS is essentially complete above $\sim 2.8\text{ mJy}$ (Condon et al. 1998) and in our final sample we apply a radio flux density cut of 3 mJy.

3.2 Redshift distributions

The radio-loud subsets of the three LRG samples may not have the same redshift distribution as their parent sample. In

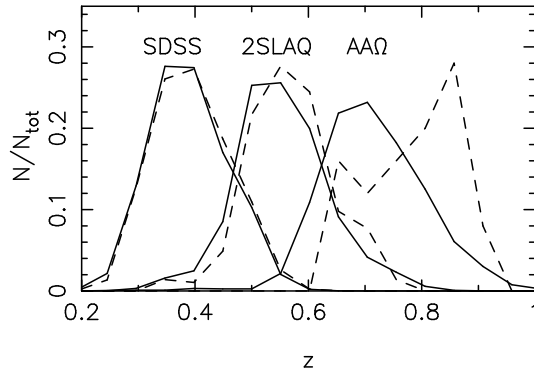


Figure 1. The solid lines shows the redshift distributions of the SDSS, 2SLAQ and AA Ω spectroscopic samples (left to right). The dashed lines show the redshift distribution of those objects identified as radio sources. These are, in general, identical to the parent distribution. In the highest redshift AA Ω sample there is a difference, but there are only 17 objects defining this distribution.

Fig. 1 we plot the redshift distribution of the spectroscopic LRG samples, and those objects that we identify as radio galaxies from our matching routine.

For the SDSS and 2SLAQ samples it is clear that the radio-detected subsamples have an identical redshift distribution to their parent samples. The AA Ω radio sample shows indications of being at a higher redshift. However, there are only 17 spectroscopic AA Ω radio LRGs and hence the distribution is highly uncertain. For the rest of this paper we will assume that the radio LRGs have the same redshift distribution as their parent sample. None the less, if the indication of Fig. 1 is accurate (that the radio LRGs have a higher redshift than the parent sample) this will effect our results. In particular a cross correlation between the radio loud sample and the parent sample will be reduced if the redshift distributions do not overlap so well.

4 CORRELATION ANALYSIS

To study the clustering of the samples defined above we calculate the 2-point angular correlation function to measure the LRG \times LRG autocorrelations and the LRG \times radio cross correlation. The 2-point angular correlation function is defined as the relative increase in pair counts at a given scale over that of a random sample. That is

$$w(\theta) = \frac{N(R)}{N(D)} \frac{DD(\theta)}{DR(\theta)} - 1 \quad (1)$$

where DD gives the number of sample-sample pairs and DR gives the sample-random pairs at separation θ . The expression is normalised by the number density of randoms $N(R)$ divided by the density of the sample $N(D)$. In an autocorrelation the data-data pairs come from the same sample, in a cross correlation they come from differing samples. Other estimators for $w(\theta)$ (Hamilton 1993; Landy & Szalay 1993) give equivalent results for this analysis.

We constructed our random catalogue from the DR7 masks published on the SDSS website. The full DR7 area was then cut down to the area covered by FIRST and populated with random sources with a density twenty times that of the radio LRGs.

4.1 Error estimation

Standard Poisson errors are notoriously inaccurate for correlation functions due to the high level of covariance in the data (e.g. Sawangwit et al. 2009). More often bootstrap or field-to-field errors are employed as an independent measure of the precision of the results. We calculate field-to-field errors by subdividing our sample into nine declination strips that contain even numbers of objects in our random catalogues. We calculate the correlation function within each field and the error is estimated by the rms of the correlation functions in each field divided by three.

5 CORRELATION FUNCTIONS

In Fig. 2 we show the LRG-LRG and LRG-radio (hereafter L×L and L×R) angular correlation functions for the three samples we are studying. In the top panels we show the raw correlations. In the bottom panels we show the ratio of our measurements to the best double power-law fit to the L×L correlation function taken from Sawangwit et al. (2009).

In all three samples we study it is apparent that the L×R correlation is stronger than the L×L autocorrelation, indicating that radio galaxies are found preferentially in richer environments than their parent LRG population. The L×R cross correlation (like L×L) exhibits a clear inflection at intermediate scales (\sim a few arcmin) which is generally interpreted as the crossover between the intra and inter-halo scales. Similar to previous authors we find that the excess clustering signal from the L×R correlation is strongest in the 1 halo regime. Donoso et al. (2009) interpret this as indicating radio galaxies hold a particularly central position within their dark matter halo. At larger scales the difference between the L×L and L×R correlation functions is reduced, and becomes negligible above ~ 20 arcmin in the AA Ω sample. As we discuss later this may be due to the radio sources being brighter in this higher-redshift sample.

To relate the measured angular correlation function, $w(\theta)$, to the 3D spatial correlation function, $\xi(r)$, we follow the standard approach outlined in Phillipps et al. (1978). Given the clear inflection in the correlation functions shown in Fig. 2 we assume the spatial correlation function can be parametrised as a double power law and integrate equation 13 from Phillipps et al. (1978) to give $w(\theta)$. In our analysis we fix the break scale in the correlation function to $1 h^{-1}$ Mpc. We fit for the slopes of the two power laws and the amplitude of the large-scale power law. Table 1 gives the parameters of fits to the observed data.

The large scale slope of $\xi(r)$ in the L×R data is essentially identical in each sample, as it is when compared to the L×L correlations. The small scale power law is considerably steeper in the radio correlations indicating that the local environment of radio LRGs is more overdense compared to the environment external to its own dark matter halo.

5.1 Radio loud vs. quiet LRG clustering

Radio galaxies are known to be found preferentially in the most luminous host galaxies (e.g. Mauch & Sadler 2007). The most luminous galaxies tend to also be found in the highest density regions and following previous authors (e.g.

Table 1. Parameters of power-law fits to the L×L and L×R angular correlation functions. The first columns are taken from (Sawangwit et al. 2009). The fits are shown in Fig. 2.

Sample	L×L		L×R	
	$r_0(h^{-1} \text{ Mpc})$	γ	$r_0(h^{-1} \text{ Mpc})$	γ
SDSS	7.35 ± 0.08	2.19 ± 0.03	7.46	2.31 ± 0.07
	9.15 ± 0.16	1.85 ± 0.04	9.48 ± 0.21	1.79 ± 0.08
2SLAQ	6.32 ± 0.03	2.16 ± 0.01	6.27	2.32 ± 0.04
	7.78 ± 0.05	1.85 ± 0.02	9.13 ± 0.17	1.82 ± 0.06
AA Ω	5.96 ± 0.03	2.14 ± 0.01	5.06	2.49 ± 0.05
	7.84 ± 0.04	1.81 ± 0.02	8.71 ± 0.18	1.83 ± 0.07

Wake et al. 2008) we test whether this covariance is responsible for the increased L×R correlation strength. We construct random samples of LRGs from our parent catalogues that have the same (r -band) magnitude and $r-i$ colour distributions as the radio LRG catalogues. In Fig. 2 we show the cross correlation between this matched catalogue and the full LRG sample. We find that they follow the L×L lines almost exactly indicating that the host mass/luminosity is not the single factor that defines the probability that a LRG is a radio source, there must be an environmental effect as well.

Our results are in agreement with most previous authors (Wake et al. 2008; Mandelbaum et al. 2009; Donoso et al. 2009). Hickox et al. (2009), on the other hand, finds that the radio galaxies in his sample cluster with the same amplitude as galaxies matched in terms of their optical properties. They note that the result is marginal but also point out that their radio galaxies have considerably higher stellar mass to radio power ratios than the other samples, and suggest this as a potential explanation for the discrepancy. Certainly if the clustering strength depends on the radio luminosity that could potentially explain their result.

5.2 Clustering strength vs. radio luminosity

Prestage & Peacock (1988) found that less luminous FR1 objects tended to be in overdense regions while more luminous FR2s had a clustering environment similar to the overall population of radio-quiet galaxies. However, many authors (e.g. Peacock & Nicholson 1991; Magliocchetti et al. 2004) have found no relationship between radio power and large scale clustering strength. Donoso et al. (2009) found variations in the correlation amplitude with radio power that were more pronounced at smaller spatial scales. At these smaller scales they found that the correlation amplitude increased with radio power up to $\sim 10^{25}$ W/Hz, above which the correlation amplitude flattened and then began to fall again above $\sim 10^{25.5}$ W/Hz.

We divide our sample of radio LRGs into three bins of roughly equal size by their flux density with cuts at $S_{1.4 \text{ GHz}} = 5$ and 20 mJy/Hz . Fig. 3 shows the L×R cross correlations for each of the flux density bins for the three LRG samples.

We do not find the same behaviour in each LRG sam-

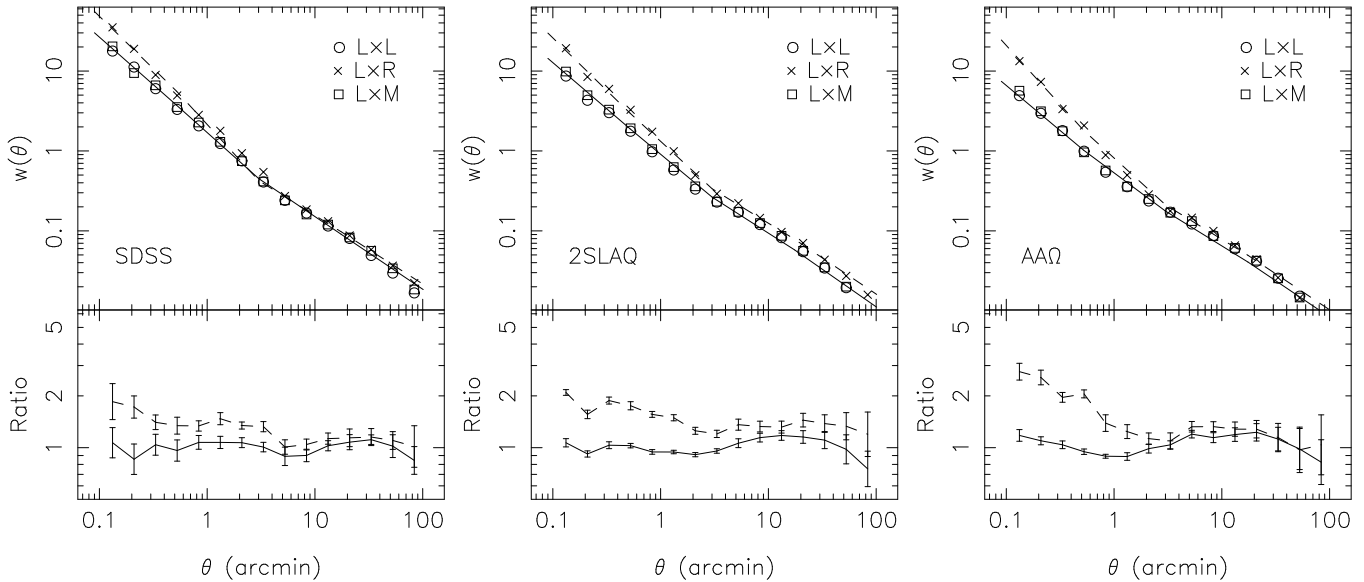


Figure 2. The L×L and L×R correlation functions for the SDSS, 2SLAQ and AAΩ samples (left to right). Also shown is the L×M cross correlation of the sample matched to the radio samples in terms of optical luminosity and colour. The top panels show the correlation functions along with best fit models to the L×M (solid) and L×R (dashed) data. The models are double power laws in $\xi(r)$ mapped to $w(\theta)$ with Limber’s equation. The bottom panels show the ratio of the L×R and L×M correlations to the best fit L×L model. Errorbars are omitted from the top plots for clarity.

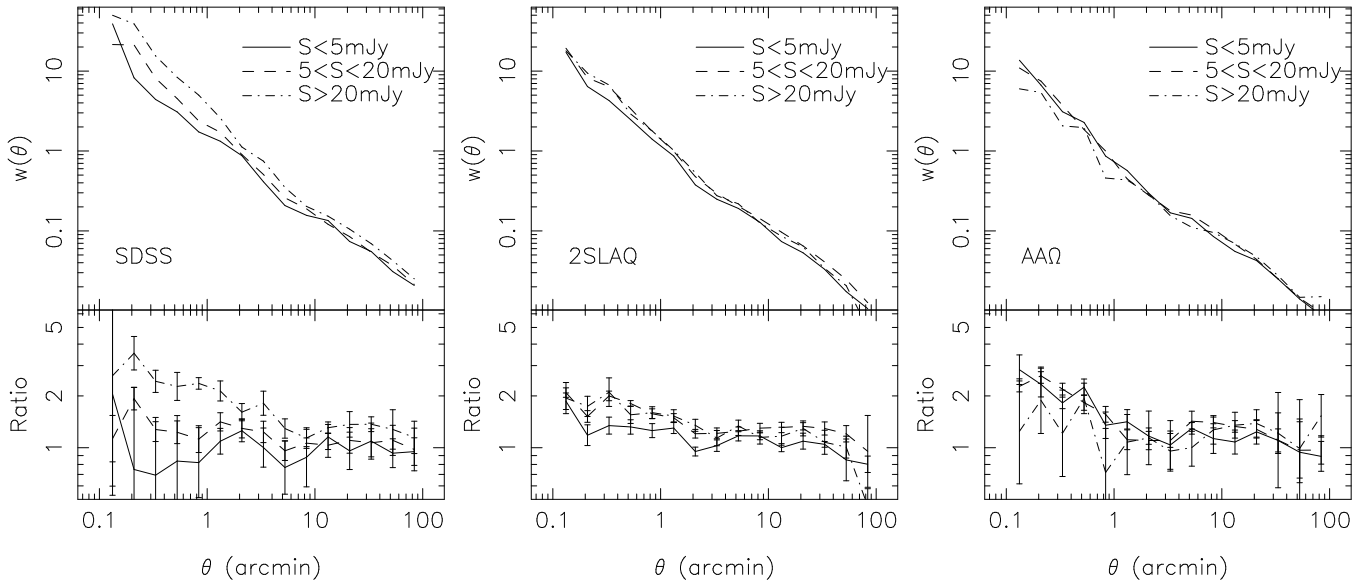


Figure 3. L×R cross correlation functions for the SDSS, 2SLAQ and AAΩ samples (left to right) with the radio sample split into three bins by radio flux density. The bottom panels show the ratio of the correlation functions to the best fit L×L model. Errorbars are omitted from the top plots for clarity. In the SDSS sample there is evidence for a positive correlation between radio flux density and the correlation strength. This is not so clear in the other two samples.

ple. In the SDSS sample there is a clear positive correlation between radio luminosity and the angular correlation amplitude. As with the difference between the L×L and L×R correlations, the luminosity dependence is most pronounced at small angular scales (< 2 arcmin). In the 2SLAQ sample the lowest flux density bin is significantly ($> 3\sigma$) lower than the other two subsets that essentially lie on top of each other. However, in the highest redshift AAΩ sample we find no significant difference between the three flux bins.

Our results are broadly consistent with those of Donoso et al. (2009). At the median redshift of our samples the flux density limits we have chosen 5/20 mJy correspond to $\log(L_{1.4\text{ GHz}}/(W/\text{Hz})) = 24.3/24.9, 24.7/25.3$ and $25.0/25.5$ for the SDSS, 2SLAQ and AAΩ samples respectively. Hence our results are consistent with the small-scale radio correlation function increasing for radio luminosities $\lesssim 10^{25}$ W/Hz and then flattening off.

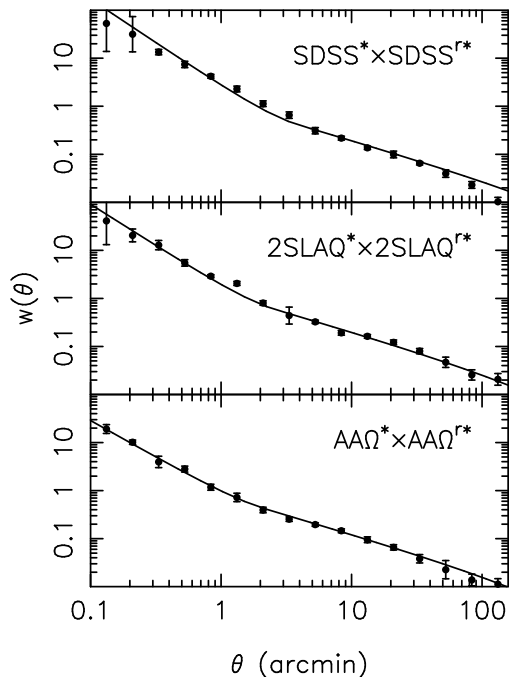


Figure 4. The $\text{SDSS}^* \times \text{SDSS}^{r*}$, $2\text{SLAQ}^* \times 2\text{SLAQ}^{r*}$ and $\text{AA}\Omega^* \times \text{AA}\Omega^{r*}$ cross correlation functions. The solid lines show the best-fit double power laws in $\xi(r)$ mapped to $w(\theta)$ with Limber’s equation.

6 CLUSTERING STRENGTH OF RADIO SOURCES AT $Z < 0.68$

Given our three samples span $z \sim 0.68$ to 0.35 (~ 2.3 Gyr of cosmic time) we are interested in any signs of evolution in the clustering strength of radio LRGs. To make a fair comparison we make our samples as equivalent as possible in terms of their optical and radio selection. Sawangwit et al. (2009) showed that by applying magnitude limits of $i_{dev} = 19.32$ and 20.25 to the 2SLAQ and AA Ω samples respectively, they could be made roughly equivalent to the SDSS sample in terms of their (optical) luminosity distribution and space density (given that the LRG luminosity function does not evolve strongly over this interval; e.g. Wake et al. 2008). They call these optical LRG samples with additional magnitude cuts SDSS^* , 2SLAQ^* and $\text{AA}\Omega^*$. In addition, we increase the radio flux limit of the SDSS^* and 2SLAQ^* samples to 13.8 and 4.9 mJy respectively, in order to be equivalent to a radio power of $\sim 10^{24.72}$ W/Hz at the median redshift of each sample. This results in 3576, 4755, 5089 objects in our radio matched samples we will call SDSS^{r*} , 2SLAQ^{r*} and $\text{AA}\Omega^{r*}$.

In Fig. 4 we show the cross correlations between the radio matched and optically matched samples along with a best-fit double power law in $\xi(r)$ mapped to $w(\theta)$ with Limber’s equation. Again the break in the power law is assumed to be at $1h^{-1}$ Mpc when performing the fit, in addition to which we fix the slope of the large-scale power law to be $\gamma = 1.8$ to facilitate comparisons of the clustering amplitude.

Fig. 5 shows the large-scale ($> 1h^{-1}$ Mpc) clustering amplitude as a function of redshift (squares). The results are

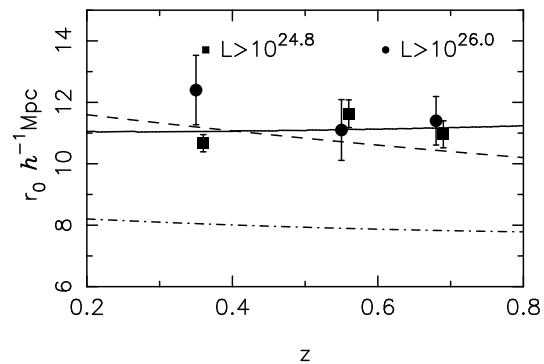


Figure 5. The large-scale cross-correlation amplitude for the $\text{SDSS}^* \times \text{SDSS}^{r*}$, $2\text{SLAQ}^* \times 2\text{SLAQ}^{r*}$ and $\text{AA}\Omega^* \times \text{AA}\Omega^{r*}$ correlations (squares) and the $\text{SDSS}^* \times \text{SDSS}^{26*}$, $2\text{SLAQ}^* \times 2\text{SLAQ}^{26*}$ and $\text{AA}\Omega^* \times \text{AA}\Omega^{26*}$ correlations (circles; these have been offset horizontally for clarity). Neither show any evidence for a trend with redshift. The lines show models for the cross-correlation amplitude based on differing assumptions about the radio-source autocorrelation. The solid and dashed lines are constant dark halo mass and long lived models respectively, fit to the lower luminosity (square) points. The dot-dashed line assumes that the radio autocorrelation is the same as that measured for quasars.

consistent with a constant clustering amplitude with little evidence for evolution.

To make a comparison with previous work on the clustering of radio sources we calculate the radio LRG two-point autocorrelation function in each sample and show the results in Fig. 6. The lines in the figure show the best fit power law in $\xi(r)$ (γ fixed to 1.8) mapped to $w(\theta)$ with Limber’s equation. Table 2 summarises the results of our power law fitting in this section.

Brand et al. (2005) measured the clustering strength of low-luminosity radio galaxies at $z \sim 0.3$ and found $r_0 = 6.1 \pm 1.1 h^{-1}$ Mpc assuming $\xi(r) = (r/r_0)^{-1.8}$. This is significantly ($\sim 3.1\sigma$) less than the value of $r_0 = 11.0 \pm 1.2 h^{-1}$ Mpc found by Peacock & Nicholson (1991) at $z < 0.1$. Brand et al. (2005) explained some of the discrepancy by assuming the clustering amplitude would increase accordingly with linear theory from $z = 0.3$ to 0. Wake et al. (2008) derived an autocorrelation clustering strength (extrapolated from the cross correlation) of $r_0 = 12.3 \pm 1.2 h^{-1}$ Mpc for radio sources in the 2SLAQ sample.

In Fig 7 we show the values for r_0 calculated in this paper (circles) along with the values found by Peacock & Nicholson (1991) (triangle), Brand et al. (2005) (square) and Wake et al. (2008) (star). A best fit to these points gives a gradient consistent with zero ($< 0.5\sigma$).

The flux limits of the Peacock & Nicholson (1991) and (Wake et al. 2008) samples are such that they sample < 2 times fainter in terms of radio luminosity at their median redshifts compared to our samples. Hence, these surveys are sampling relatively bright objects where we do not find clustering strength correlating with radio power (Fig. 3). The Brand et al. (2005) sample on the other hand goes ~ 6.5 times fainter. This difference may explain why their result is lower than the other values.

Table 2. Parameters of power law fits to the angular correlation function for samples matched in terms of their optical and radio properties. Samples included are denoted * (optically selected LRGs), r^* (radio LRGs with $L_{1.4\text{GHz}} > 10^{24.72}$ W/Hz) and 26^* (radio LRGs with $L_{1.4\text{GHz}} > 10^{26}$ W/Hz).

Correlation	SDSS		2SLAQ		AA Ω	
	$r_0(h^{-1}\text{Mpc})$	γ	$r_0(h^{-1}\text{Mpc})$	γ	$r_0(h^{-1}\text{Mpc})$	γ
$* \times r^*$	4.55	2.81 ± 0.09	5.07	2.72 ± 0.08	5.49	2.53 ± 0.06
	10.67 ± 0.28	1.8	11.63 ± 0.45	1.8	10.96 ± 0.44	1.8
$r^* \times r^*$	10.4 ± 1.6	1.8	11.9 ± 1.3	1.8	11.6 ± 1.3	1.8
$* \times 26^*$	10.67 ± 1.13	1.8	11.63 ± 0.99	1.8	10.96 ± 0.79	1.8

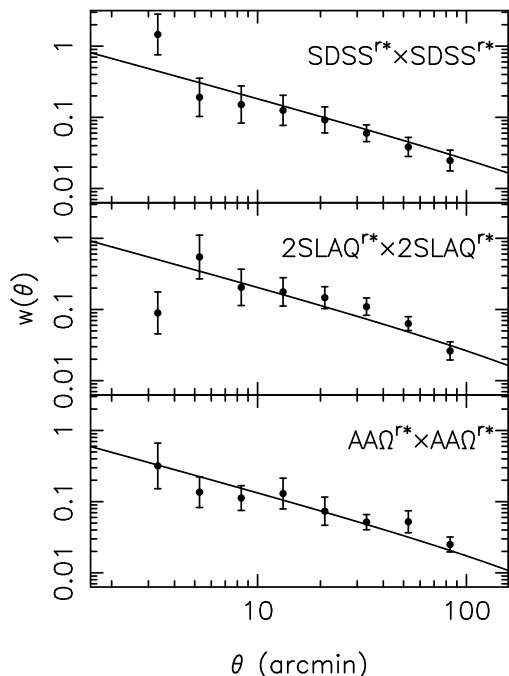


Figure 6. Autocorrelation functions for the three samples after they have been made approximately equivalent in terms of their optical and radio selection. The solid line gives the best fit relation in terms of $\xi(r) = (r_0/r)^\gamma$ propagated through Limber's formula.

6.1 Evolution of the clustering amplitude of radio galaxies

It is clear from Fig. 7 and the squares in Fig. 5 that there is little evidence for evolution in the clustering amplitude of either the auto or cross correlation with redshift. Fitting $r_0 \propto (1+z)^\alpha$ to the measurements in Fig. 7 (excluding the Brand et al. 2005 point) gives $\alpha = 0.20 \pm 0.30$. The same fit for the cross correlation (squares in Fig. 5) gives $\alpha = 0.23 \pm 0.21$. In addition we fit a series of physically motivated models to our data:

(i) In linear theory structures evolve as $\xi_m \propto D^2(z)$ where $D(z)$ is the growth factor and ξ_m is the matter correlation function. Structures that grow according to this have a constant bias (b) where $b^2 = \xi/\xi_m$. In Fig. 7 we fit a constant bias model to our data and plot the results as the dot-dashed

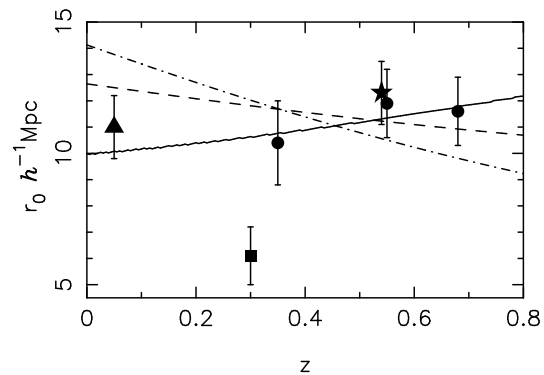


Figure 7. The radio galaxy \times radio galaxy autocorrelation amplitude r_0 as a function of redshift. The circles correspond to our three samples in addition to points from Peacock & Nicholson (1991) (triangle), Brand et al. (2005) (square) and Wake et al. (2008) (star; this point is offset horizontally for clarity). The measurements are consistent with no evolution in the clustering amplitude with redshift up to $z \sim 0.68$. The Brand et al. (2005) point is significantly offset from the rest, potentially due to their sample being dominated by fainter objects. The lines give three model fits to the data excluding the Brand et al. (2005) point. The models are constant dark halo mass (solid), long-lived (dashed) and linear growth (dot-dashed).

line. This model is only marginally consistent with our data ($\chi^2 = 11.11$; $P(\chi^2, \nu = 4) \sim 2.5\%$).

(ii) We further include the long-lived model of Fry (1996) that assumes no change in the comoving number density of galaxies and that clustering grows solely due to gravitational effects. The long lived model has been shown to describe evolution in the LRG \times LRG correlation function (Sawangwit et al. 2009). Fits to the radio cross and auto correlation amplitudes are shown as dashed lines in Figs. 5 and 7. Note that the long-lived model does not require that radio sources themselves exist for cosmological timescales. Rather that the dark matter halos that host them evolve passively under the influence of gravity. This model involves little evolution and hence gives a better fit to our data.

(iii) We also fit a model in which dark halo mass is held constant with redshift (solid lines Figs. 5 and 7; see Sawangwit et al. 2009 for our formalism for relating bias to dark halo mass). This type of model has been shown to fit the evolution of the quasar autocorrelation function over $0 \lesssim z \lesssim 2.5$.

To relate our models for the radio auto correlation to the cross correlation amplitudes in Fig. 5 we assume the LRG clustering follows the best-fit long-lived model from Sawangwit et al. (2009). We then assume that the cross-correlation of two samples (ξ_{12}) is related to the two autocorrelations (ξ_{11} and ξ_{22}) by (e.g. Wake et al. 2008)

$$\xi_{12}^2 = \xi_{11}\xi_{22}. \quad (2)$$

The long-lived and constant mass models fit our data acceptably ($P(\chi^2, \nu) > 10\%$) with the exception of the long-lived model fit to the cross correlation results. In this case we find $\chi^2 = 9.08$ with $P(\chi^2, \nu = 2) \sim 1.1\%$ indicating that the long-lived model may not accurately describe radio source clustering. The dark halo masses derived for the radio sources are 9.4 and $5.6 \times 10^{13} h^{-1} M_\odot$ for the cross and auto correlation respectively.

The offset in the derived dark halo masses may be due to equation 2 not holding in our data. In this paper and Sawangwit et al. (2009) large-scale correlation amplitudes have been calculated for the $* \times *$ LRG auto correlation, $* \times *r$ cross correlation and the $*r \times *r$ autocorrelation. Calculating the cross correlation amplitude from the autocorrelations and equation 2 gives $r_0 = 9.75 \pm 0.75$, 10.28 ± 0.56 and $10.26 \pm 0.58 h^{-1}$ Mpc for the SDSS, 2SLAQ and $AA\Omega$ samples respectively. These values are consistently lower than the amplitudes measured from the cross correlation, although only by ~ 1 to 2σ . Taking the three samples together the offset is $\sim 3\sigma$. The offset may be due to two causes. First, the fits are not completely equivalent; we fit double power laws over a larger range of θ for the $* \times *$ and $* \times *r$ correlations. Second, equation 2 assumes a linear bias model that may not hold in this case.

7 CLUSTERING OF LUMINOUS RADIO SOURCES AT $Z < 0.68$

The SDSS^{r*}, 2SLAQ^{r*} and $AA\Omega^{r*}$ samples are dominated by objects below the $\sim 10^{26}$ W/Hz divide between brighter FRI and FRII sources. 10^{26} W/Hz is also roughly the divide between radio AGN host galaxies that show no emission lines and those that do. Furthermore, above $\sim 10^{26}$ W/Hz radio sources show strong number density evolution, more similar to quasars. The clustering strength of quasars evolves weakly with redshift (Croom et al. 2005; Ross et al. 2009). In this section we use our sample to test for evolution in the clustering amplitude of bright radio LRGs.

A radio luminosity of 10^{26} W/Hz corresponds to flux limits of ~ 266 , 95 and 57 mJy at $z \sim 0.35$, 0.55 and 0.68 respectively. Cutting back our samples to these limits leave 49, 224 and 283 objects in what we will call the SDSS^{26*}, 2SLAQ^{26*} and $AA\Omega^{26*}$ samples. These are not large enough to calculate an autocorrelation amplitude so we calculate the two-point cross correlation with the corresponding (starred) LRG catalogues. Fig. 8 shows the cross correlations along with best fit solutions to $\xi(r) = (r_0/r)^{1.8}$ propagated through Limber's formula. In Fig. 5 the circles show r_0 for these bright objects as a function of redshift.

Note that while lower-luminosity radio AGN are typically found in LRGs with red stellar spectra, the brightest sources can be found in both broad and narrow emission-line objects that have younger stellar populations (e.g.

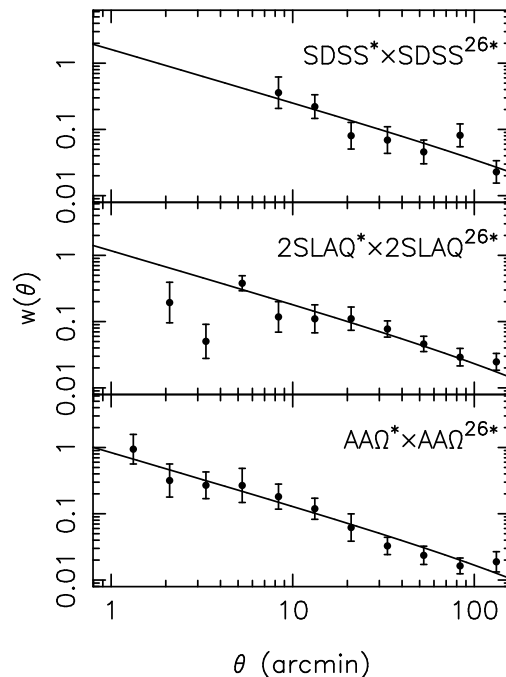


Figure 8. The SDSS^{*}×SDSS^{26*}, 2SLAQ^{*}×2SLAQ^{26*} and $AA\Omega^{*}$ × $AA\Omega^{26*}$ cross correlation functions. The solid line shows the best fit solutions to $\xi(r) = (r_0/r)^{1.8}$ propagated through Limber's formula.

Johnston et al. 2008). Hence, while an LRG selection finds most hosts of radio galaxies in the range $10^{23} < L < 10^{26}$ W/Hz, above this there is a significant population of blue objects that may be missed by the optical selection.

7.1 Evolution of the clustering amplitude of luminous radio sources

As with the less luminous sample, we find very little evidence for evolution in the clustering amplitude of these brightest radio sources. Fitting the cross correlation points (circles Fig. 5) for $r_0 \propto (1+z)^\alpha$ gives $\alpha = -0.38 \pm 0.52$.

We also compare our results for the clustering of the brightest radio sources with that of quasars. To do this we assume all quasars cluster such that their derived dark halo mass is $3 \times 10^{12} M_\odot$ at all redshifts (Croom et al. 2005; Ross et al. 2009) and work backwards to derive the clustering strength as a function of redshift. We then convert this to a cross-correlation clustering strength making the assumptions discussed above. We plot the derived value for the cross-correlation amplitude in Fig. 5 as the dot-dashed line.

While our derivation is approximate it suggests that the clustering amplitude of bright radio sources may evolve slowly with redshift and in an almost luminosity-independent manner, similar to the results found for quasars. There is also strong evidence that the objects in our sample cluster considerably more strongly than quasars, as previously noted for fainter radio sources. The implication is that these bright radio sources must inhabit considerably denser regions of space and correspondingly more massive dark matter halos compared to quasars. There is less difference between the large-scale clustering environment of lu-

minous and faint radio sources. However, the small scale $r < 1h^{-1}\text{Mpc}$ clustering environment of the brightest radio sources appears significantly denser than the environment of the faintest sources. This may indicate the effect of the radio source on its immediate surroundings, given that the larger-scale environment is luminosity independent.

8 CONCLUSIONS

We have cross-matched three large photometric samples of LRGs to the FIRST and NVSS surveys to define three samples of radio LRGs. We have then measured the 2-point correlation function to investigate the clustering properties of the samples. Similar to previous authors we find evidence that: 1) radio LRGs are more strongly clustered than non-radio galaxies matched in terms of luminosity and colour; 2) the clustering strength of radio LRGs at $r < 1h^{-1}\text{Mpc}$ increases with radio luminosity up to $L \sim 10^{25}\text{ W/Hz}$ and then remains roughly constant but at $r > 1h^{-1}\text{Mpc}$ the clustering is independent of radio luminosity. We further find that inconsistencies between the radio-LRG cross-correlation and auto-correlation amplitudes may suggest that a simple linear bias model may be insufficient to describe the relation between radio-LRG and/or LRG clustering and mass clustering.

However, the primary goal of this work was to investigate any evolution in the clustering strength of radio galaxies with redshift. We find no evidence for evolution in the large scale ($r > 1h^{-1}\text{Mpc}$) clustering amplitude of radio-LRGs. We show that our radio \times radio LRG autocorrelations are consistent with previous authors indicating no evolution in comoving coordinates in the redshift range $0 < z < 0.68$ ($\sim 6\text{Gyr}$). Furthermore, we make use of cross-correlations to increase the precision of our results and still find no evidence for evolution. We then restrict our samples to objects with $L > 10^{26}\text{ W/Hz}$ and again find no evidence for evolution in the correlation amplitude. Our results are consistent with a single dark halo mass of $9 \times 10^{13}h^{-1}\text{ M}_{\odot}$ for all radio LRGs in the redshift range $0 < z < 0.68$. This could be compared to quasars that appear to inhabit halos of $m_{\text{DH}} = 3 \times 10^{12}h^{-1}\text{ M}_{\odot}$ again reasonably independent of redshift and luminosity. The significantly more massive halos for the high-luminosity radio galaxies, at least, may provide a problem for unified AGN models. Finally, our radio-LRG cross-correlations are inconsistent with a model in which LRG clustering follows a long-lived model and radio sources are randomly sampling the LRGs.

REFERENCES

- Abazajian K. N., et al., 2009, *ApJS*, 182, 543
 Adelman-McCarthy J. K., et al., 2007, *ApJS*, 172, 634
 Becker R. H., White R. L., Gregg M. D., Brotherton M. S., Laurent-Muehleisen S. A., Arav N., 2000, *ApJ*, 538, 72
 Bell E. F., et al., 2004, *ApJ*, 608, 752
 Best P. N., Kauffmann G., Heckman T. M., Ivezić Ž., 2005, *MNRAS*, 362, 9
 Blake C., Wall J., 2002, *MNRAS*, 329, L37
 Brand K., Rawlings S., Hill G. J., Tufts J. R., 2005, *MNRAS*, 357, 1231
 Brown M. J. I., et al., 2007, *ApJ*, 654, 858
 Cannon R., et al., 2006, *MNRAS*, 372, 425
 Clewley L., Jarvis M. J., 2004, *MNRAS*, 352, 909
 Condon J. J., Cotton W. D., Greisen E. W., Yin Q. F., Perley R. A., Taylor G. B., Broderick J. J., 1998, *AJ*, 115, 1693
 Croom S. M., et al., 2005, *MNRAS*, 356, 415
 Croom S. M., et al., 2009, *MNRAS*, 399, 1755
 Donoso E., Best P. N., Kauffmann G., 2009, *MNRAS*, 392, 617
 Dunlop J. S., Peacock J. A., 1990, *MNRAS*, 247, 19
 Eisenstein D. J., et al., 2001, *AJ*, 122, 2267
 Fanaroff B. L., Riley J. M., 1974, *MNRAS*, 167, 31P
 Fry J. N., 1996, *ApJL*, 461, L65+
 Hamilton A. J. S., 1993, *ApJ*, 417, 19
 Hickox R. C., et al., 2009, *ApJ*, 696, 891
 Hine R. G., Longair M. S., 1979, *MNRAS*, 188, 111
 Johnston H. M., Sadler E. M., Cannon R., Croom S. M., Ross N. P., Schneider D. P., 2008, *MNRAS*, 384, 692
 Kimball A. E., Ivezić Ž., 2008, *AJ*, 136, 684
 Landy S. D., Szalay A. S., 1993, *ApJ*, 412, 64
 Longair M. S., 1966, *MNRAS*, 133, 421
 Magliocchetti M., et al., 2004, *MNRAS*, 350, 1485
 Mandelbaum R., Li C., Kauffmann G., White S. D. M., 2009, *MNRAS*, 393, 377
 Mauch T., Sadler E. M., 2007, *MNRAS*, 375, 931
 McCarthy P. J., 1993, *ARAA*, 31, 639
 Peacock J. A., Nicholson D., 1991, *MNRAS*, 253, 307
 Phillipps S., Fong R., Fall R. S. E. S. M., MacGillivray H. T., 1978, *MNRAS*, 182, 673
 Prestage R. M., Peacock J. A., 1988, *MNRAS*, 230, 131
 Ross N. P., Shanks T., Cannon R. D., Wake D. A., Sharp R. G., Croom S. M., Peacock J. A., 2008, *MNRAS*, 387, 1323
 Ross N. P., et al., 2009, *ApJ*, 697, 1634
 Sadler E. M., et al., 2007, *MNRAS*, 381, 211
 Sawangwit U., et al., 2009, *ArXiv e-prints*
 Schmidt M., 1968, *ApJ*, 151, 393
 Wake D. A., Croom S. M., Sadler E. M., Johnston H. M., 2008, *MNRAS*, 391, 1674
 Wake D. A., et al., 2006, *MNRAS*, 372, 537
 Wake D. A., et al., 2008, *MNRAS*, 387, 1045
 Yates M. G., Miller L., Peacock J. A., 1989, *MNRAS*, 240, 129
 York D. G., et al., 2000, *AJ*, 120, 1579